M.R. Ghanbarpour, K.C. Abbaspour, G. Jalalvand, and G.A. Moghaddam – Stochastic modeling of surface stream flow at different time scales: Sangsoorakh karst basin, Iran. *Journal of Cave and Karst Studies,* v. 72, no. 1, p. 1–10. DOI: 10.4311/jcks2007ES0017

STOCHASTIC MODELING OF SURFACE STREAM FLOW AT DIFFERENT TIME SCALES: SANGSOORAKH KARST BASIN, IRAN

M. Reza Ghanbarpour[1]*, Karim C. Abbaspour[2], Goudarz Jalalvand[3], and Ghodsieh Ashtiani Moghaddam[1]

Abstract: Karstic watersheds are one of the most important areas for water supply. Because the role of groundwater contribution to surface water flow in karst watersheds is not well understood, the commonly used hydrologic models in most regular basins do not provide satisfactory estimates of runoff in karstic regions. This paper uses time-series analysis to model karstic flow in the Sangsoorakh karst drainage basin in the Karkheh subbasin of southwest Iran. The comparison of model forecasting performance was conducted based upon graphical and numerical criteria. The results indicate that autoregressive integrated moving average (ARIMA) models perform better than deseasonalized autoregressive moving average (DARMA) models for weekly, monthly and bimonthly flow forecasting applications in the study area.

Introduction

Accurate simulation and forecasting of water availability is a key step in efficient planning, operation, and management of water resources. Developing reliable surface water flow forecasting methods for real-time operational water resources management becomes increasingly important. Various approaches, including physical and mathematical models, have been used for this purpose. The problem is more complicated in karstic basins due to the nature of the dynamic processes involved. Therefore, karstic basins should be considered distinct from other drainage areas (LeGrand, 1973). As Graupe et al. (1976) noted, karstic basins respond differently to rainfall than do non-karstic drainage areas in such a way that a part of the precipitation is often stored in underground storage spaces that discharges at springs after a delay and long after the rainfall has ceased. Hence, surface hydrology rules and relationships that are valid in non-karstic watersheds have a more complex situation in karstic basins.

Similarities of karstic aquifers to surface networks and their consistency throughout the whole of the karst drainage network are generally unknown (Glennon and Groves, 2002). Discrete recharge to a karst aquifer occurs through openings such as sinkholes. Karst aquifers recharged in this manner typically have numerous inputs of surface water to the subsurface with water draining along cracks, fissures, and zones of weakness in soluble bedrock (Lerch et al., 2005). Because karstic flow networks occur underground, karst drainage basins possess complex boundaries and inexact and sometimes unknown subsurface flow routes. Limestone basins behave differently from normal surface stream systems because of the nature of the underground drainage (Jakeman et al., 1984). Therefore, the commonly used surface hydrology models, such as curve number or rational method, which provides satisfactory estimates of runoff in most regular basins, may not provide accurate results in karstic regions.

Schomberg et al. (2005) analyzed 72 ungauged, agricultural watersheds in Minnesota and Michigan using the hydrologic model SWAT to determine the effects of land use and surficial geology on stream flow, sediment, and nutrients. Some streams in those watersheds are influenced by karst topography. They found seasonal and annual differences in flow and nutrient and sediment loading across different land forms and land use types. Jourde et al. (2007) analyzed the contribution of karst groundwater to surface water flow using a hydrologic model. They found that the model was unable to replicate recorded flood hydrographs at both the upstream (non-karstic watershed) and downstream (karstic watershed) gauging stations.

Time-series analysis (Box and Jenkins, 1976) has been widely used in the field of hydrology and water resources for simulation and forecasting (Hipel and McLeod, 1994). Time-series analysis provides effective tools for selecting a model that describes the historical time series behavior. Selected models could be used to forecast future events. Studies have shown that stochastic time-series models are very useful within the field of complex karstic flow systems, when detailed information are not available (Graupe et al., 1976; Jakeman et al., 1984; Dimitrov et al., 1997). The behavior and the response function of the karstic system can be characterized by autoregressive models, spectral and cross correlation analyses, and transfer function noise. Autoregressive stochastic methods have been used by Ozis

* Corresponding Author
[1] Faculty of Natural Resources, Sari Agricultural Sciences and Natural Resources University, P.O.Box: 737, Sari, Iran, m_ghanbarpour@yahoo.com
[2] Swiss Federal Institute for Aquatic Science and Technology, EAWAG, Ueberlandstr, 133, P.O. Box 611, 8600 Duebendorf, Switzerland
[3] Lar consulting company, Sharifi Street, No. 23, Tehran, Iran

and Keloglu (1976) for flow simulation in karstic basins in Turkey. In these basins, karstified limestone formations are predominant. In most basins, daily and monthly first order autoregressive models were the most appropriate stochastic models. Graupe et al. (1976) used an autoregressive model and moving average for simulating and forecasting flow in karstic basins. In their research, Graupe et al. found that the first order autoregressive model for partial karstic basins and second order autoregressive model for complete karstic basins were identified as the best models. A mathematical overview of single and cross correlation and spectral analyses was presented by Mangin (1984). Dimitrov et al. (1997) also used time series stochastic models including autoregression on the dependent variable as well as on the residuals and multiple regression using different time lags in a karstic basin in Bulgaria. In this basin, the limestone thickness varied within the range 20–250 m. The average elevation of the basin was about 800–1000 m. The Upper Cretaceous limestone is highly karstified and both surface and underground karst forms exist. They concluded that the stochastic linear differential equation with independent error process was the best approach for flow estimation when detailed information on the rainfall-runoff processes is not available. Mathevet et al. (2004) analyzed the hydrological functioning of a karst system using some time-series analysis methods including correlation and spectral analyses and noise and wavelet analyses. The non-stationary and timescale-dependent behavior of the system was studied.

The objective of this research was to develop and compare two stochastic models for flow forecasting in the Sangsoorakh karst basin located in the Karkheh sub-basin in southwest Iran. The models are based on a seasonal autoregressive integrated moving average (ARIMA) and a deseasonalized autoregressive moving average (DARMA). For this study, stochastic approaches were used to develop weekly, monthly, and bi-monthly flow simulation and forecasting models.

METHODS AND MATERIALS

STUDY AREA

The Sangsoorakh karst drainage basin covers an area of 53.4 km^2 in the Karkheh subbasin in southwest Iran (Fig. 1). The highest elevation of the basin is 3498 m in southeastern portion and the lowest is 1760 m in the northeastern portion. The average rainfall is 636 mm yr^{-1} (Jalalvand, 1999). The average annual discharge of the basin at the hydrometric station is 4.2 m^3 s^{-1}. The estimated runoff coefficient is about 0.32 (Jalalvand, 1999). The average monthly temperature is 6.1 °C with a minimum of −7.5 °C in December and a maximum of 19.0 °C in August. The soil in the area is mountainous with shallow depth and light texture (sandy) and with plenty of stones and gravels. This area is covered by natural rangeland especially near Sarab-Gamasyab Spring (Fig. 2). Most parts of the basin are karstic

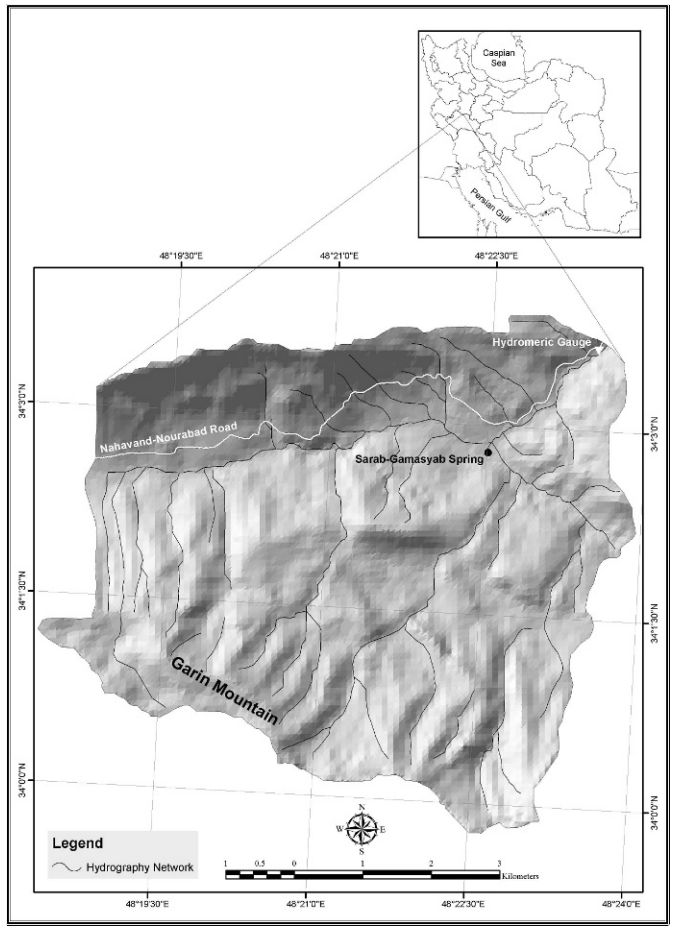

Figure 1. Location of Sangsoorakh Basin in the Karkheh Basin in western Iran.

(Jalalvand, 1999). Flow simulation and forecasting is very important in the study area for management of water resources, estimation and prediction of spring floods, and for water supply planning. Furthermore, increasing the relative accuracy for flow forecasting in high- and low-flow seasons for efficient water resources management has special economic values.

DATA

The data collected in this study consisted of weekly, monthly, and bimonthly flow rates, which were measured using a hydrometric gauge at the outlet of the basin. The data period for this study was for the water years of 1979–80 to 2003–04. A split sample procedure was used for calibration and validation. In each of the weekly, monthly, and bi-monthly databases, flow data from 1979–80 to 1997–98 were used for calibration and data from 1998–99 to 2003–04 for validation.

GEOLOGY OF THE BASIN

This area is located in the overthrusted Zagros zone. It is an intensely fractured and faulted narrow band found between Sanandaj-Syrjan and the folded Zagros zones

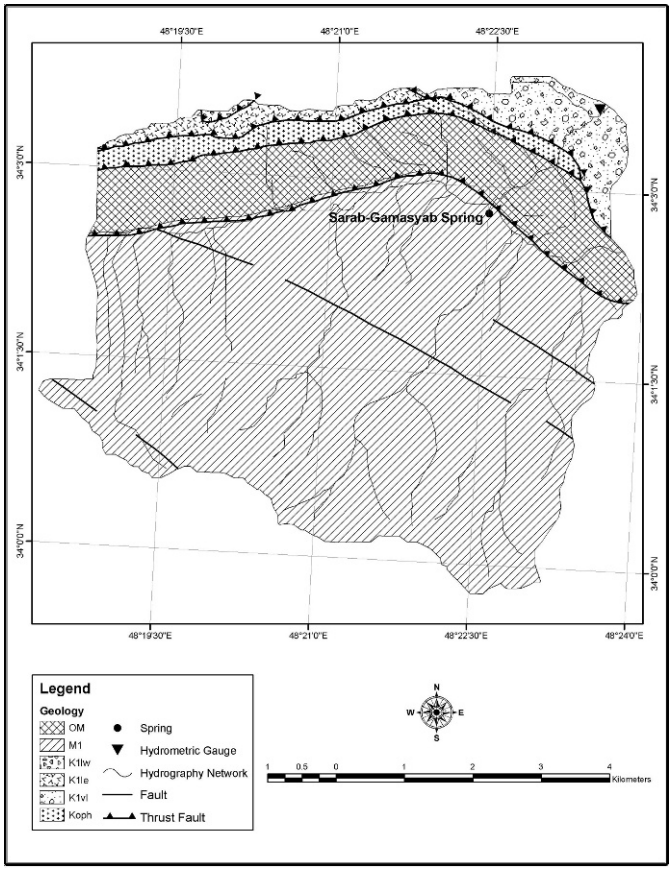

Figure 2. Sangsoorakh geology map and its karstic formations (Jalalvand, 1999).

(Fig. 2). The top part of region is mainly covered by sedimentary and metamorphic rocks. Sedimentary rocks consist of karstic limestone and conglomerates. Metamorphic formations mostly consist of crystallized limestone and low-grade metamorphic shale that are white-gray to dark-gray in color, and in some cases, there are lime-marl to marl layers. Geomorphic activities have created many clay and calcite filled pores.

In Figure 2, the first geologic unit, Cretaceous rocks from oldest to youngest are indicated as K1vl, K1le, K1lw. K1lv is a pyroclastic member that consists of crystallized limestone and volcanic rocks. As shown in Figure 2, these rocks cover most of the northern region around the basin outlet. The second member, K1le, consists of carbonate rocks such as weathered microsparite and dolomicrite in various shades of gray color in the north and northwestern part of the region. Therefore, it can be said that these are an indicator facie among other facies. K1lw is a thick to massive member that is crystallized white limestone and is located in northwestern part of the region. According to the Nahavand geological map (1:100,000), all these members belong to the lower Cretaceous period (Jalalvand, 1999).

The second unit is ophiolite that is exposed along Garin Mountain in Nahavand-Nourabad road. It is about 10-km-long and more than 200-m-wide. It is the main outcrop in the basin and consists of red plugic limestone and radiolarian cherts within basaltic volcanic rocks. This unit has been covered by Oligo-Miocene deposits.

Tertiary deposits of Oligo-Miocene age cover 80 percent of the basin, and consist of OM and M1 members. OM is a kind of tectonic thrusted member that is composed of sand, shale, and siltstone with thin layers of gray limestone. As a result of faulting, bedding slopes in varying directions, and in some places, are near vertical. The limestone has many microfossil traces. The thickness of micro-conglomerates is about 10 m and consists of shale, crystallized limestone, and old sandstone. The microfossils were studied in a thin carbonate layer and were found to belong to upper-Oligocene and lower-Miocene units (Jalalvand, 1999).

M1, which is located in the southern part of Garin Mountain, is 360–400-m-thick and composed of biomicrite carbonate rocks with many microfossil traces. There are many macropores in this unit caused by infiltrating surface water and dissolution of limestone, which led to the creation of a karstic environment. In addition, canyons, clints, and avens are some other forms of karst morphology that exist in this unit.

Time Series Analysis

Time-series models can be used to describe the stochastic structure of a hydrologic data series. In this study, the ARIMA (Box and Jenkins, 1976) and the DARMA (Hipel and McLeod, 1994) models were used to model weekly, monthly, and bimonthly flow time series.

The ARIMA model is constructed using a combination of moving average (MA) and autoregressive (AR) processes, after differencing the data to remove nonstationarity. For the nonseasonal component of a seasonal ARIMA model, the MA operator is written as

$$\theta(B) = 1 - \theta_1 B - \theta_2 B^2 - \ldots - \theta_q B^q \qquad (1)$$

where q is the order of the nonseasonal MA operator, θ_j, $j = 1, 2, \ldots, q$, are the MA parameters, and B is the backward shift operator such that $BZ_t = Z_{t-1}$. The AR operator is written as

$$\phi(B) = 1 - \phi_1 B - \phi_2 B^2 - \ldots - \phi_p B^p \qquad (2)$$

where p is the order of the nonseasonal AR operator, and ϕ_i, $i = 1, 2, \ldots, p$, are the nonseasonal AR parameters. The nonseasonal ARIMA model for a set of equispaced measurements, $Z = \{Z_1, Z_2, \ldots, Z_n\}$, can be written as

$$\phi(B)(1-B)^d(Z_t) = \theta(B)a_t \qquad (3)$$

where d is the number of differences, t is discrete time, and a_t is the white noise series which has a finite variance and a mean of zero. Differencing removes nonstationarity in a time series. When differencing is not required, the model is referred to as an ARMA model. Construction of ARIMA models is conducted based on the three stages of model

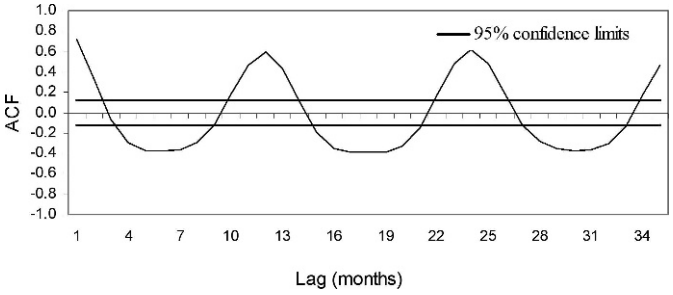

Figure 3. ACF for the monthly flow data series for the Sangsoorakh Hydrometric Station.

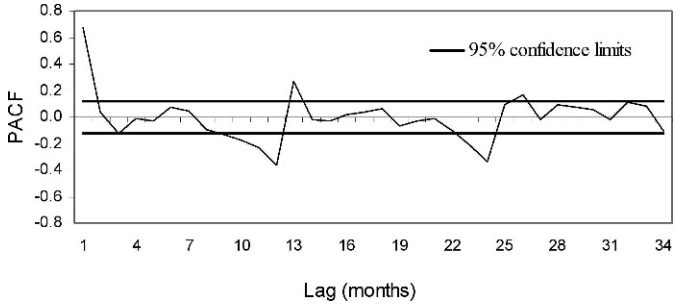

Figure 5. PACF for the seasonally differenced monthly flow data series for the Sangsoorakh Hydrometric Station.

building: identification, estimation, and diagnostic checking, which is discussed in detail by Hipel et al. (1977). The 95% confidence limits are calculated using

$$Var[p_k] \cong \frac{1}{N}\left(1+2\sum_{i=1}^{q} p_i^2\right) \qquad \text{for } (k>q) \qquad (4)$$

under the assumption that p_k is zero for all nonzero lag and N is length of the data series

The nonseasonal ARIMA model in Equation (3) can be expanded to the seasonal case by adding seasonal differencing, as well as seasonal MA and AR operators to produce the seasonal ARIMA model defined as

$$\phi(B)\Phi(B^s)(1-B)^d\,(1-B^s)^D\,(Z_t-\mu)=\theta(B)\Theta(B^s)a_t \qquad (5)$$

for which

1. the seasonal length is s (s = 12 for monthly data),
2. $(1-B^s)^D$ is the seasonal differencing operator of order D,
3. $\Theta(B^s)=1-\Theta_1 B^s-\Theta_2 B^{2s}-\ldots-\Theta_Q B^{Qs}$ is the seasonal MA operator of order Q,
4. Θ_i is the ith seasonal MA parameter,
5. and $\Phi(B^s)=1-\Phi_1 B^s-\Phi_2 B^{2s}-\ldots-\Phi_p B^{Ps}$ is the seasonal AR operator of order P where Φ_i is the ith seasonal AR parameter.

The notation $(p,d,q)(P,D,Q)_s$ is used to represent the seasonal ARIMA model in Equation (5). The three entries within the first set of parentheses stand for the orders of the nonseasonal AR, differencing, and MA operators, respectively, while the three numbers contained inside the second set of parentheses give the orders of the seasonal AR, differencing, and MA operators, respectively. Finally, prior to fitting the seasonal ARIMA model in Equation (6) to the Z_t time series, the series may first be transformed by a Box-Cox transformation, for which a logarithmic transformation is a special case, to eliminate problems with nonnormality and heteroscedasticity in the estimated model residuals (Hipel and McLeod, 1994).

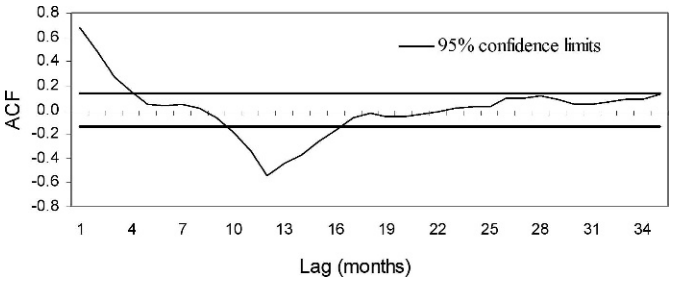

Figure 4. ACF for the seasonally differenced monthly flow data series for the Sangsoorakh Hydrometric Station.

The second stochastic method, DARMA is a widely used approach to model seasonal data series. In this method, first the series should be deseasonalized and then an appropriate nonseasonal stochastic model fit to the deseasonalized data. Two standard deseasonalization techniques that have been widely used are

$$w_{i,j}=Z_{i,j}^{\lambda}-\bar{\mu}_j \qquad (6)$$

and

$$w_{i,j}=\frac{\left(Z_{i,j}^{\lambda}-\bar{\mu}_j\right)}{\bar{\sigma}_j} \qquad (7)$$

where $Z_{i,j}$ is the transformed observation for the ith year, jth month, μ_j is the fitted mean for season j, σ_j is the fitted standard deviation for season j, and the superscript λ is the exponent of an appropriate Box-Cox transformation (Hipel and McLeod, 1994). After the series are deseasonalized, nonseasonal ARMA models are fitted to the data. Finally, the notation DARMA (p,q) is employed to represent this type of deseasonalized model where p and q stand for the orders of the nonseasonal and seasonal AR and MA operators presented in Equations (2) and (1), respectively.

Calibration of time-series models is conducted based on the three stages of model building: identification, estimation, and diagnostic checking (Box and Jenkins, 1976; Hipel et al., 1977; Hipel and McLeod, 1994). The purpose of the identification stage is to determine the differencing required to produce stationarity and the persistence structure in the series using interpretation of the autocorrelation function

Table 1. Selected ARIMA models and the model parameters.

Time Interval	Model	Model Parameters					
		p_1	p_2	p_3	q_1	P_1	Q_1
Weekly	$ARIMA(3,0,0)(0,1,1)_{52}$	0.885	⋯	⋯	0.089	0.062	0.687
	$ARIMA(3,0,1)(0,1,1)_{52}$	0.885	⋯	0.662	−0.009	−0.384	1.345
	$ARIMA(2,0,0)(0,1,1)_{52}$	0.888	⋯	⋯	⋯	0.124	0.698
	$ARIMA(1,0,0)(0,1,1)_{52}$	0.890	⋯	⋯	⋯	⋯	0.798
Monthly	$ARIMA(1,0,0)(0,1,1)_{12}$	0.889	⋯	⋯	⋯	⋯	0.594
	$ARIMA(1,0,1)(0,1,1)_{12}$	0.890	⋯	0.138	⋯	⋯	0.684
	$ARIMA(2,0,1)(0,1,1)_{12}$	0.890	⋯	−0.772	⋯	0.552	−0.220
	$ARIMA(3,0,1)(0,1,1)_{12}$	0.885	⋯	−0.733	−0.005	0.537	−0.182
Bimonthly	$ARIMA(1,0,1)(1,1,1)_6$	0.876	−0.185	−0.193	⋯	⋯	0.387
	$ARIMA(1,0,0)(1,1,1)_6$	0.875	−0.201	⋯	⋯	⋯	0.526
	$ARIMA(2,0,1)(1,1,1)_6$	0.877	−0.185	−0.523	⋯	0.185	0.057
	$ARIMA(2,0,0)(1,1,1)_6$	0.875	−0.191	⋯	⋯	−0.056	0.557

The notation $(p,d,q)(P,D,Q)_s$ is used to represent the seasonal ARIMA model in which p, d and q are order of the nonseasonal AR, differencing and MA operators respectively. P, D and Q are the order of the seasonal AR, differencing and MA operators and s is number of season per year.

(ACF) and the partial autocorrelation function (PACF). In the estimation stage, the approximate maximum likelihood estimates (MLEs) for the model parameters is obtained by employing the unconditional sum of squares method, as suggested by Box and Jenkins (1976). The third stage of time-series analysis consists of diagnostic checking of the estimated model residuals and is used to evaluate the ARIMA and DARMA models performance. To determine whether the residual are white noise and normally independently distributed, residual autocorrelation function (RACF) tests (Hipel et al., 1977) are employed. The Akaike information criteria (*AIC*) (Akaike, 1974) and Schwars' approximation of the Bayes Information Criterion (*BIC*) (Schwars, 1978) were utilized to select the most appropriate model from the candidate set of calibrated models

$$AIC = -2Ln(ML) + 2K \tag{8}$$

$$BIC = -2Ln(ML) + KLn(n) \tag{9}$$

where ML is maximum likelihood, K is the number of adjustable parameters, and n is the length of the time series. The optimal model is chosen to minimize the *AIC* or *BIC* criterion, depending on which criterion is selected.

Table 2. Selected DARMA models and the model parameters.

Time Interval	Model	Model Parameters			
		$p1$	$p2$	$p3$	$q1$
Weekly	$DARMA(3,0)$	0.686	0.065	0.077	⋯
	$DARMA(2,1)$	1.256	−0.324	⋯	0.571
	$DARMA(1,1)$	0.854	⋯	⋯	0.178
	$DARMA(1,0)$	0.789	⋯	⋯	⋯
Monthly	$DARMA(1,1)$	0.671	⋯	⋯	0.161
	$DARMA(1,0)$	0.562	⋯	⋯	⋯
	$DARMA(2,1)$	−0.131	0.543	⋯	−0.846
	$DARMA(2,0)$	0.498	0.112	⋯	⋯
Bimonthly	$DARMA(1,1)$	0.335	⋯	⋯	−0.224
	$DARMA(1,0)$	0.503	⋯	⋯	⋯
	$DARMA(2,1)$	−0.066	0.22	⋯	−0.624
	$DARMA(2,0)$	0.538	−0.068	⋯	⋯

The notation (p,q) is used to represent the deseasonalized ARMA model in which p *and* q are order of the nonseasonal AR and MA operators respectively.

For validation of the models, one-step-ahead forecasts for the test portion of the time series were generated using the selected set of calibrated models. Plotting the observed and estimated data series for each model could be used as an indication of reliability of the models at the validation stages. The forecasting performance of all the models at the validation stage was compared based on the mean absolute error (MAE), root mean square error (RMSE), and Nash-Sutcliffe efficiency (NSE) (Nash and Sutcliffe, 1970), as defined in Equations 10, 11 and 12. The procedure having lower MAE and RMSE values can be assumed to be the most accurate model for flow forecasting in the study area. NSE values equal to 1 indicate a perfect fit between simulated and observed data. An NSE value of 0 indicates that the model predictions are not acceptable (Motovilov et al., 1999). To investigate the models' overall forecasting performance at the verification stage, the coefficients of determination (R^2) were considered. R^2 indicates the strength of fit between observed and forecasted stream flow and it has the range of values between 0 and 1.

$$MAE = \frac{1}{n}\sum_{i=1}^{n}[X_{Oi} - X_{Ei}] \tag{10}$$

Table 3. Comparison of the selected ARIMA models.

Time Interval	Model	Comparison Criteria		
		AIC	*BIC*	RACF
Weekly	$ARIMA(3,0,0)(0,1,1)_{52}$	153.6	429.6	Residuals are normally distributed
	$ARIMA(3,0,1)(0,1,1)_{52}$	154.1	435.1	Residuals are normally distributed
	$ARIMA(2,0,0)(0,1,1)_{52}$	159.03	430.4	…
	$ARIMA(1,0,0)(0,1,1)_{52}$	171.5	438.03	…
Monthly	$ARIMA(1,0,0)(0,1,1)_{12}$	−22.3	35.9	…
	$ARIMA(1,0,1)(0,1,1)_{12}$	−22.3	39.3	Residuals are normally distributed
	$ARIMA(2,0,1)(0,1,1)_{12}$	−24.5	40.6	Residuals are normally distributed
	$ARIMA(3,0,1)(0,1,1)_{12}$	−22.3	46.2	Residuals are normally distributed
Bimonthly	$ARIMA(1,0,1)(1,1,1)_{6}$	−2.02	32.83	Residuals are normally distributed
	$ARIMA(1,0,0)(0,1,1)_{6}$	−2.59	26.9	Residuals are normally distributed
	$ARIMA(1,0,1)(0,1,1)_{6}$	−1.64	30.53	…
	$ARIMA(2,0,1)(0,1,1)_{6}$	−3.24	34.54	…

$$RMSE = \sqrt{\frac{1}{n}\sum_{i=1}^{n}[X_{Oi} - X_{Ei}]^2} \quad (11)$$

$$NSE = \left(1 - \frac{\sum\left(X_{Oi} - X_{Ei}\right)^2}{\sum\left(X_{Oi} - \overline{X_{Oi}}\right)^2}\right) \quad (12)$$

where n is number of data observations, X_{Oi} is observed value, X_{Ei} is estimated value, and $\overline{X_{Oi}}$ is the average of observed values.

RESULTS AND DISCUSSION

Weekly, monthly, and bimonthly stochastic ARIMA and DARMA models were developed using a time-series analysis procedure for the basin under study. To determine the autocorrelation structure in the series, we plotted the ACF and PACF that reflect linear dependence among observations separated by different time lags. As an example, the ACF for the monthly flow is illustrated in Figure 3. The ACF follows an attenuating sine wave pattern. Examination of this function revealed that the data have seasonality, which requires removal using one order of seasonal differencing.

Figures 4 and 5 show the ACF and PACF, respectively, for the seasonally differenced monthly flow-time series. As

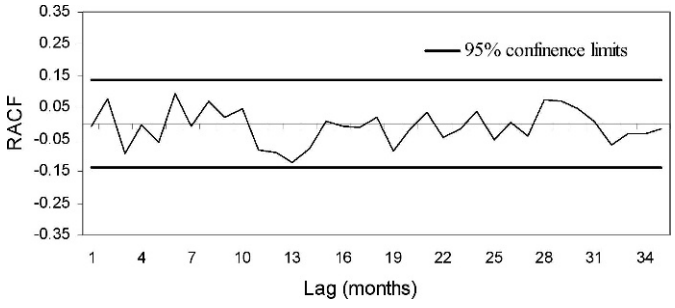

Figure 6. RACF for the selected $ARIMA(1,0,1)(0,1,1)_{12}$ monthly model for the Sangesourakh Hydrometric Station.

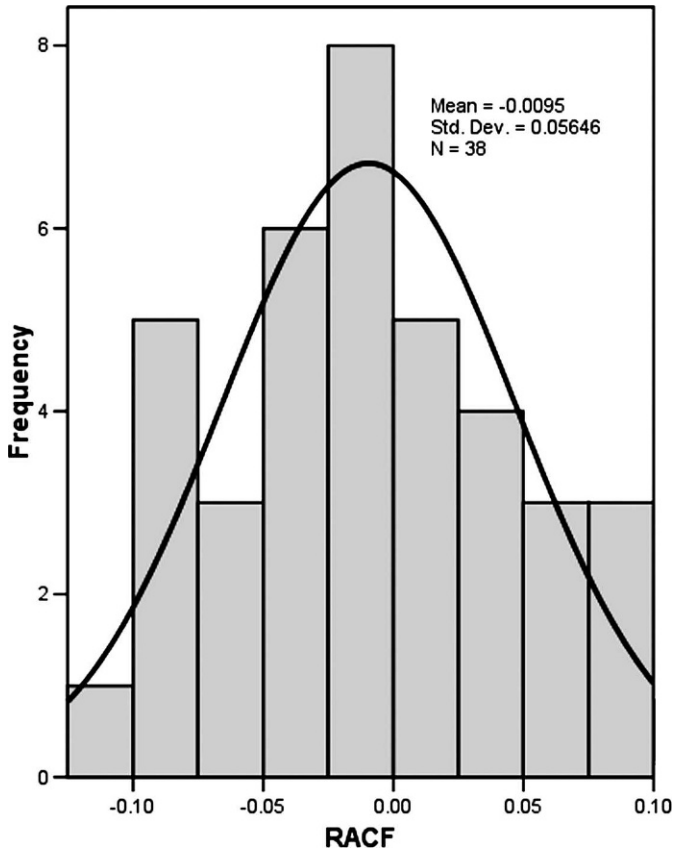

Figure 7. Plot of the residuals (RACF) of $ARIMA(1,0,1)(0,1,1)_{12}$ monthly model with normal curve.

Table 4. Comparison of the selected DARMA models.

Time Interval	Model	Comparison Criteria		
		AIC	*BIC*	RACF
Weekly	*DARMA*(3,0)	−120.05	−100.66	Residuals are normally distributed
	DARMA(2,1)	−120.29	−100.91	…
	DARMA(1,1)	−119.07	−104.5	Residuals are normally distributed
	DARMA(1,0)	−104.94	−95.25	…
Monthly	*DARMA*(1,1)	−83.25	−72.96	Residuals are normally distributed
	DARMA(1,0)	−82.89	−76.03	…
	DARMA(2,1)	−83.5	−69.84	…
	DARMA(2,0)	−83.8	−73.53	Residuals are normally distributed
Bimonthly	*DARMA*(1,1)	−316.39	−308.34	Residuals are normally distributed
	DARMA(1,0)	−317.48	−312.12	…
	DARMA(2,1)	−314.94	−304.21	…
	DARMA(2,0)	−315.96	−307.91	…

evident in Figure 4, the ACF did not truncate but rather damps out, suggesting that a nonseasonal AR parameter was needed in the model. Because the PACF truncated after lag 1 (Fig. 5), one nonseasonal AR parameter should be included in the model. There was a significant value at lag 12 that indicated the presence of a seasonal MA term in the model. In a similar way, all possible models were identified for data series at the other time scales. Table 1 presents the four selected ARIMA models for the weekly, monthly, and bimonthly flow in the study area.

For the case of DARMA models, all flow-time series were deseasonalized. For weekly data, flows were deseasonalized using the estimated means of the series (Equation (6)). For monthly data, it was necessary to use both Equations (6) and (7), but for bimonthly data, flows were first transformed using natural logarithms and then deseasonalized using Equation (6). Then, the three mentioned modeling stages of time-series analysis were followed to calibrate the DARMA forecasting models. Deseasonalized models are useful for describing time series in which the mean and variance within each season are stationary across the year. Table 2 presents four selected DARMA models which might be suitable for simulating flow time series at different time scales.

Table 5. Summary of the performance analysis of forecasting models.

Time Interval	Model	*MAE*	*RMSE*	*NSE*	R^2
Weekly	ARIMA	1.41	1.82	0.49	0.52
	DARMA	1.46	1.89	0.43	0.50
Monthly	ARIMA	1.25	1.57	0.61	0.54
	DARMA	1.29	1.68	0.56	0.60
Bimonthly	ARIMA	1.24	1.5	0.62	0.56
	DARMA	1.23	1.56	0.59	0.59

The approximate maximum likelihood (MLE) estimates for the model parameters were obtained by employing the unconditional sum of squares method suggested by Box and Jenkins (1976). Model parameters for ARIMA and DARMA models are shown in Table 1 and 2, respectively. For checking the adequacy of the models fitted to the time series, residual autocorrelation function (RACF) tests were employed. The *AIC* and *BIC* were used to select the best fit model out of the various competing models.

Table 3 shows the comparison between all ARIMA models based on RACF, *AIC*, and *BIC*. With respect to these criteria, the $ARIMA(3,0,0)(0,1,1)_{52}$ model performs better than the other three weekly models. For the monthly and bimonthly flow series, $ARIMA(1,0,1)(0,1,1)_{12}$ and $ARIMA(1,0,1)(1,1,1)_6$ are more accurate. A plot of the RACF for the selected $ARIMA(1,0,1)(0,1,1)_{12}$ model is shown in Figure 6. From Figure 6, it can be noted that the estimated values fall within the 5% significance interval. The residuals were white noise and normally distributed (Figure 7).

A comparison of all DARMA models is shown in Table 4. Based on the mentioned diagnostic criteria, *DARMA*(1,1) were selected as the most reliable weekly, monthly, and bimonthly DARMA models, respectively.

One-step-ahead forecasts for the verification part of the weekly, monthly, and bimonthly flow (1998–99 to 2003–04)

Table 6. Statistical comparison of the forecasting models using paired-sample *t*-test analysis.

Model Time Interval	*t*	Degrees of Freedom	Significance
Weekly	−1.732	259	0.084
Monthly	−10.188	59	0.00
Bimonthly	6.457	29	0.00

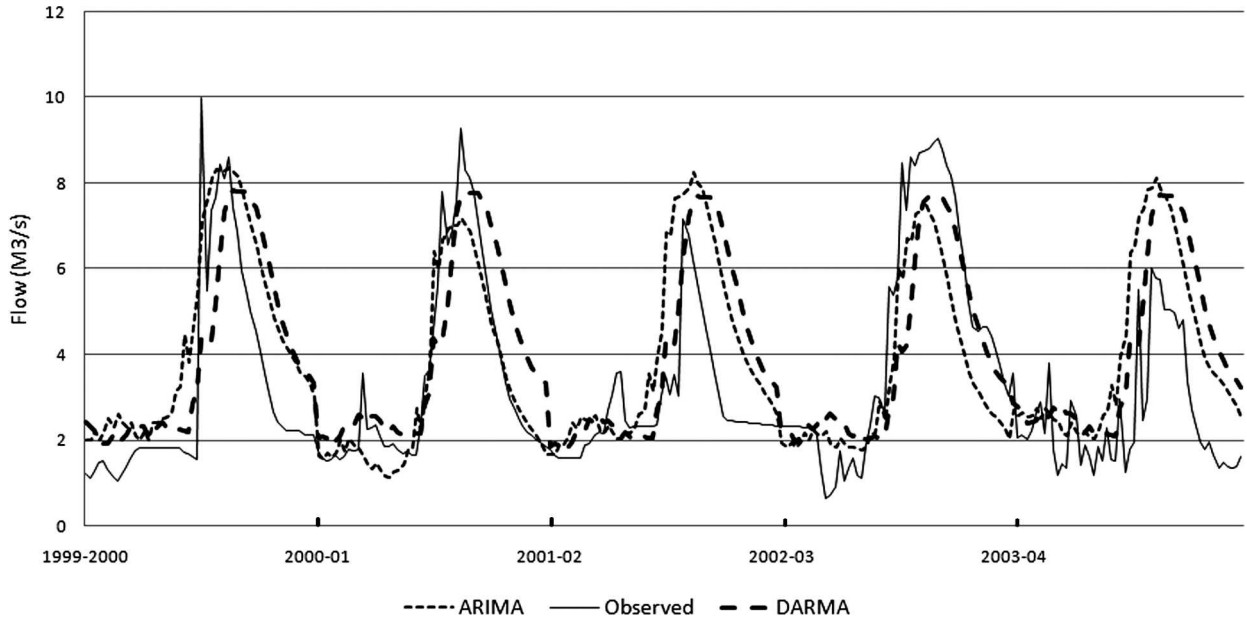

Figure 8. Comparison of observed and forecasted weekly flow using ARIMA and DARMA models for validation period (1999–00 to 2003–04).

were generated using the selected set of the ARIMA and DARMA models. The resulting calibrated models were then examined for use in predicting flow data series at the three different time scales.

We used the validation data sets to compare the forecasting ability of the ARIMA and DARMA models. Table 5 gives the indices used to compare the goodness of model simulation for weekly, monthly, and bimonthly time scales.

For the case of the weekly flow forecasting, the seasonal ARIMA model provides slightly better results than DARMA in terms of MAE and RMSE. As can be seen in Table 6, the differences are significant at the 0.05 level based on a paired sample *t*-test analysis. However, the results of the monthly and bimonthly ARIMA and DARMA models were slightly similar and the differences are not significant at the 0.05 level (Table 6). The NSE was used to evaluate the simulation accuracies of the two models. The NSE of the ARIMA in comparison to the DARMA models is more satisfactory (Motovilov et al., 1999). The NSF for weekly, monthly, and bimonthly flow is 0.49, 0.61 and 0.62, respectively (Table 5).

To show the validation results of the models for weekly, monthly, and bimonthly flows, in Figures 8, 9, and 10, respectively, we plot both the observations and the predictions. As seen in Figure 8 for the weekly simulation, DARMA slightly overestimates the flow during the recession periods. Overestimation of the flow by the DARMA model during recession periods also could be seen in Figures 9 and 10. However, it could be concluded that the weekly, monthly, and bimonthly ARIMA models are more suitable than DARMA in the study area, especially for dry periods.

CONCLUSIONS

Two time-series analysis models, ARIMA and DARMA, have been used to simulate the surface water discharges in a karst basin by the identification, estimation, and diagnostic check stages of stochastic model construction (Hipel and McLeod, 1994). The main objective of this work was to provide a set of numerical comparisons between stochastic-flow simulation and forecasting models for a small karstic watershed.

As demonstrated by the simulation experiments outlined in the paper, selected ARIMA and DARMA models statistically preserve specified historical statistics. Also, diagnostic checks reveal that the normality assumptions for the residuals are fulfilled and model parsimony is preserved. Therefore, the calibrated ARIMA and DARMA models adequately simulate weekly, monthly, and bimonthly flows in the study area.

A comparison of model predictions with historical data for the period of 1979–80 to 2003–04 water years demonstrated the accuracy of the models. As indicated in this research, forecasts of flows are reasonably accurate for both of the modeling techniques. The NSE for both models at three time scales are more than 0.43 and it shows that simulation results are all satisfactory (Motovilov et al., 1999). However, it has been found that the weekly, monthly, and bimonthly ARIMA models perform better than DARMA models based on the results of the

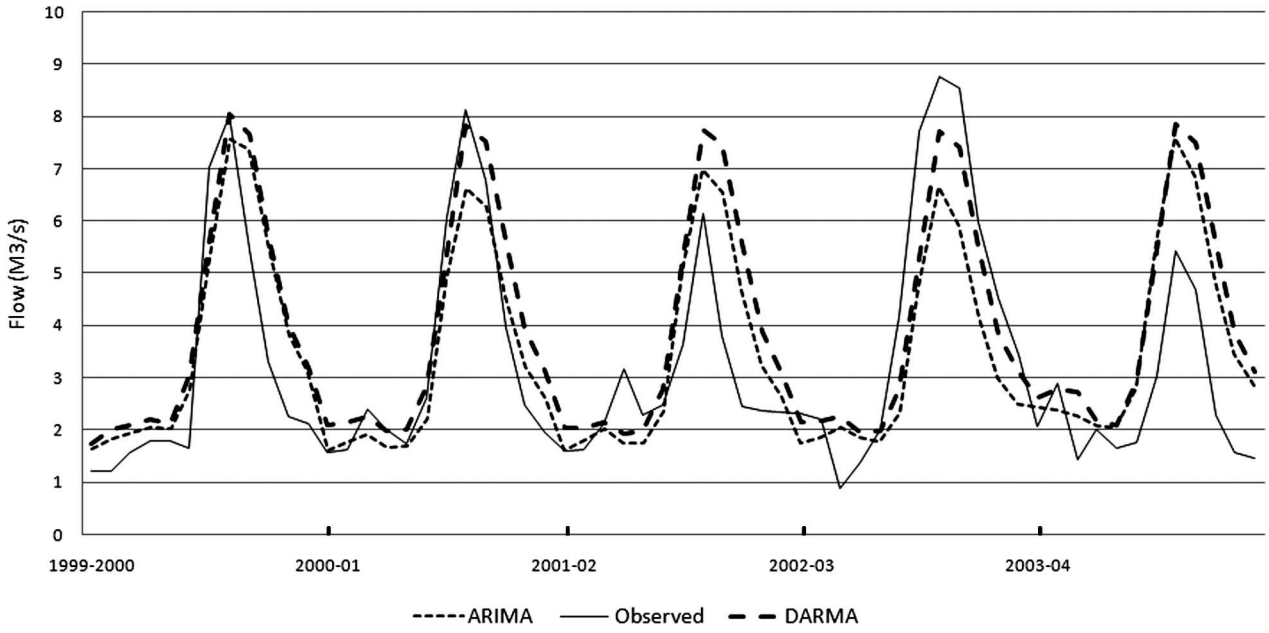

Figure 9. Comparison of observed and forecasted monthly flow using ARIMA and DARMA models for validation period (1999–00 to 2003–04).

numerical and graphical comparison of forecasting performance of the models.

The process of rainfall-runoff is more complicated in karst than non-karst basins because it has been shown in some previous studies. Schomberg et al. (2005) found that two gauges with a predicted coefficient of variation (CV) of flow greater than the actual CV of flow were in predominantly loess areas with karst influence. Predictability, constancy and CV of flow were all predicted as overly flashy by their SWAT model, which is heavily influenced by karst geology. They concluded that karst watersheds are more complex and more poorly understood

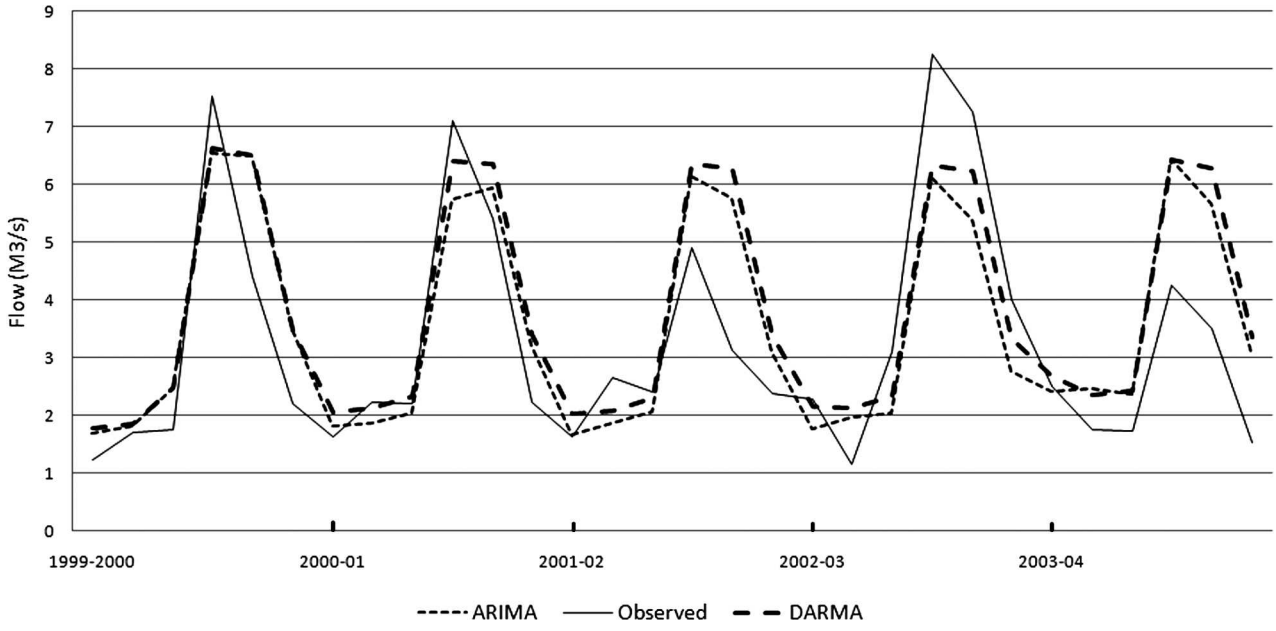

Figure 10. Comparison of observed and forecasted bimonthly flow using ARIMA and DARMA models for validation period (1999–00 to 2003–04).

than non-karst systems (Felton, 1994) and have been shown to require more specialized calibration to obtain accurate results (Spruill et al., 2000). Jourde et al. (2007) have shown that surface runoff hydrologic models cannot simulate the flow in the karstic part of the watershed under study because there is an additional contribution to surface flow from the karstic area and it is probably related to a delayed contribution of karst groundwater to surface flow. They suggest a fully coupled surface–subsurface hydrologic model to characterize the dynamics of the karst groundwater contribution to the surface drainage network.

In a karstic system, surface water flow is an observed output of the basin, which is available usually with better accuracy. As noted by Graupe et al. (1976) and Dimitrov et al. (1997), the application of stochastic models, such as the ones used in this study, offers an inexpensive solution to the operational input data, especially when insufficient spatial and temporal hydrodynamic information is available. However, more research is necessary to prove that stochastic time-series models could have better capabilities than physical models within the field of complex karstic flow systems.

ACKNOWLEDGEMENT

The authors would like to thank the referees for their very helpful comments on the manuscript.

REFERENCES

Akaike, H., 1974, A new look at the statistical model identification: IEEE Transactions on Automatic Control, v. 19, p. 716–723.

Box, G.E.P., and Jenkins, G.M., 1976, Time series analysis: Forecasting and control, revised edition, San Francisco, Holden-Day.

Dimitrov, D., Machkova, M., and Damyanov, G., 1997, On the karst spring discharge forecasting by means of stochastic modeling, *in* Gunay, G., and Johnson, A.I., eds., Karst waters & environmental impacts, Rotterdam, Balkema, p. 353–359.

Felton, G.K., 1994, Hydrologic responses of a karst watershed: Transactions of the ASAE, v. 37, p. 143–150.

Glennon, A., and Groves, C., 2002, An examination of perennial stream drainage patterns within the Mammoth Cave Watershed, Kentucky: Journal of Cave and Karst Studies, v. 64, no. 1, p. 82–91.

Graupe, D., Isailovic, D., and Yevjevich, V., 1976, Prediction model for runoff from karstified catchments, *in* Proceedings of the U.S.-Yugoslavian Symposium on Karst Hydrology and Water Resources, Dubrovnik, June 2–7, 1975, p. 277–300.

Hipel, K.W., McLeod, A.I., and Lennox, W.C., 1977, Advances in Box-Jenkins modeling, Part one, Model construction: Water Resources Research, v. 13, p. 567–575.

Hipel, K.W., and McLeod, A.I., 1994, Time series modeling of water resources and environmental systems, Amsterdam, Elsevier, 1013 p.

Jakeman, A.J., Greenway, M.A., and Jenings, J.N., 1984, Time-series models for the prediction of stream flow in a karst drainage system: Journal of Hydrology, v. 23, no. 1, p. 21–33.

Jalalvand, G., 1999, Investigation of hydro-geomorphology of Gamasiyab river basin [Ms.c. thesis], Tehran, University of Tehran, 154 p. (in Persian).

Jourde, H., Roesch, A., Guinot, V., and Bailly-Comte, V., 2007, Dynamics and contribution of karst groundwater to surface flow during Mediterranean flood: Environmental Geology, v. 51, p. 725–730.

LeGrand, H.E., 1973, Hydrological and ecological problems of karst regions: Science, v. 179, no. 4076, p. 859–864.

Lerch, R.N., Wicks, C.M., and Moss, P.L., 2005, Hydrologic characterization of two karst recharge areas in Boone County, Missouri: Journal of Cave and Karst Studies, v. 67, no. 3, p. 158–173.

Mangin, A., 1984, Pour une meilleure connaissance des systemes hydrologiques a partir des analyses correlatoires et spectrales: Journal of Hydrology, v. 67, p. 25–43.

Mathevet, T., Lepiller, M., and Mangin, A., 2004, Application of time-series analyses to the hydrological functioning of an Alpine karstic system: the case of Bange-L'Eau-Morte: Hydrology and Earth System Sciences, v. 8, no. 6, p. 1051–1064.

Motovilov, Y.G., Gottschalk, L., Engeland, K., and Rohde, A., 1999, Validation of a distributed hydrological model against spatial observations: Agriculture and Forest Meteorology, v. 98–99, p. 257–277.

Nash, J.E., and Sutcliffe, J.V., 1970, River flow forecasting through conceptual models, Part 1: A discussion of principles: Journal of Hydrology, v. 10, p. 282–290.

Ozis, U., and Keloglu, N., 1976, Some features of mathematical analysis of karst, *in* Proceedings of the U.S.-Yugoslavian Symposium on Karst Hydrology and Water Resources, Dubrovnik, June 2–7, 1975, p. 221–235.

Schomberg, J.D., Host, G., Johnson, L.B., and Richard, C., 2005, Evaluating the influence of landform, surficial geology, and land use on streams using hydrologic simulation modeling: Aquatic Sciences, v. 67, p. 528–540.

Schwars, G., 1978, Estimating the dimension of a model: Annals of Statistics, v. 6, p. 461–464.

Spruill, C.A., Workman, S.R., and Taraba, J.L., 2000, Simulation of daily and monthly stream discharge from small watersheds using the SWAT model: Transactions of the ASAE, v. 43, p. 1431–1439.